From experimental data the mechanics relationships describing the behaviour of four different low alloyed steel powders during uniaxial cold compaction

Ilaria Cristofolini[a], Alberto Molinari[a], Gianluca Pederzini[b], Alex Rambelli[b]

[a] Department of Industrial Engineering - University of Trento, Via Sommarive 9 – 38123 Trento – Italy
[b] Powder Metal B.U. - Sacmi Imola S.C., Via Provinciale Selice 17/a – 40026 Imola (BO) – Italy

Abstract

In previous works the behaviour of the powder column during uniaxial cold compaction was deeply investigated, determining the relationships describing the densification, as well as the stress field determining the constitutive model. The whole analysis was based on experimental data, and an improved processing method was defined. Main focus was on AISI 316L powder.

This work aims at applying this improved experimental method to investigate and compare the behaviour of four different commercial water atomized low alloyed steel powders. Single action experiments were performed, obtaining cylindrical specimens with different H/D ratios. The distribution of axial and radial stresses was investigated, and the relationships describing both the radial stress transmission coefficient and the flow stress as functions of the relative density were determined. The radial stress transmission coefficient also confirmed the hypothesized value of the Poisson coefficient. The friction coefficient between the powder column and the die wall was determined, also highlighting the influence of the H/D ratio. Measuring the axial and radial strains due to spring-back, the axial and radial elastic moduli were determined, as functions of the relative density. The results obtained for the four materials were compared, also highlighting both differences and similarities.

Keywords: metal powders, cold compaction, compaction model

1. Introduction

In the conventional press-and-sinter powder metallurgy process, powders are uniaxially cold compacted in rigid dies, to obtain the so-called green part. The scope of cold compaction is obtaining the maximum green density compatible with the complexity of geometry, as required by the functionality of the part. Density distribution has also to be evaluated . The compressibility of the powder determines the densification during cold compaction, and it is in turn affected by several parameters, such as chemical composition, alloying method, interstitial content, size distribution and shape. Moreover, the strategic role played by the lubricant admixed to reduce the friction between the powder and the die surface can not be neglected.

Such a friction determines an inhomogeneous axial distribution of green density along the height of the green part, due to the decrease of the compaction force in the powder column along the distance from the compaction surfaces, i.e. the surfaces in contact with the punches [1]. The peculiar characteristics of the powder mix increase the difficulty in describing the powder behaviour during cold compaction, which determines the densification. Actually, particles are subject to deformation during cold compaction, so that the real contact surface between powder column and die surface changes on increasing density. Moreover, lubricant also changes during cold compaction, due to the frictional heat, so that it more efficiently spreads over the interparticle spaces. The influence of carbon content, added as graphite, has also to be taken into account. Due to the reasons above the friction coefficient between the powder and the die surface is in principle unknown, and it has been investigated by several authors. Comparing the results of a theoretical analysis of cold compaction to experimental data, Al Qureshi et al. [2, 3] determined a friction coefficient that was assumed as constant during the compaction cycle. Nevertheless, investigating iron powder compacted in a wall lubricated die, Mosbah et al. [4] observed that the friction coefficient is a function of the relative density, constant up to 0.7 relative density, then continuously decreasing. A continuous decrease is also reported by Wikman et al. [5, 6], but the trend is reported as decreasing over the whole relative density range. The variation with density is proposed by Pavier and Doremus [7] through the dependence on the normal stress. Densification is determined by a triaxial state of stress, due to the constrain exerted by the rigid die, which opposes the expansion of the powder mix in the compaction plane [8]. Considering axi-symmetric parts, the stress field leading to densification comprehends both the stress in the axial direction (applied by the punches) and the stresses in the compaction plane (radial and tangential stresses exerted by the die). The relationship between axial and radial stress (equal to the tangential stress in cylindrical specimens) is given by the radial stress transmission coefficient, which depends on the actual density during compaction as an inherent function of the powder mix, mainly related to the interparticle friction [3, 9, 10].

Friction coefficient and stress field must thus be investigated to describe the densification behaviour and the constitutive model of the powder mix. Friction coefficient can be measured by means of different experimental methods [11],. Radial stress can also be measured, either through load cells in the die or through strain gauges on the outer surface of the die. However, all these methods require experimental devices, which are not provided on industrial presses.

In previous studies an alternative method was proposed to determine the two variables, only needing the forces and displacements continuously recorded by an industrial hydraulic press, without any additional instrument and device [9, 10, 12]. The present work exploits this method to highlight the influence of both the powder mix and the geometry on the parameters describing the stress field acting on the powder column. Four different commercial low alloyed steel powder mixes, which were used to produce specimens characterized by different H/D ratios, were investigated, also comparing the obtained results.

2. Experimental procedure

Four different commercial water atomized low alloyed powders, the composition and characteristics of which are summarized in Table 1, were studied in this work. 0.6% Kenolube as lubricant was added to all the mixes.

Table 1: Characteristics of the powders used

Material	Mo	CuMoNi	CrMo	CuMo

Composition	Fe – 0.85% Mo	Fe – 0.5% Mo – 1.5%Cu – 4%Ni	Fe – 0.5% Mo – 3%Cr	Fe – 1.5% Mo – 2%Cu
Characteristics	Pre-alloyed (Fe-0.85%Mo) powder	Fe powder, diffusion bonded with finely divided Mo (0.5%), Cu (1.5%), and Ni (4%)	Pre-alloyed (Fe-0.5%Mo-3%Cr) powder	Pre-alloyed (Fe-1.5%Mo) powder, added with 2%Cu by diffusion annealing
C content	0.2%C	0.6%C	0.55%C	0.65%C

Cylindrical specimens, 35.004 mm diameter, two different H/D ratios (0.8, 1.3), were obtained compacting the powder mixes in a rigid die using a 200 tonnes hydraulic press, equipped with 9 hydraulic and 1 electric closed-loop controlled axes.

Exploiting previous experiences [9,10,12], downwards single action compaction strategy was performed, obtained by keeping still the die. Following parameters, as shown in Figure 1, were continuously recorded during compaction: F_u, compaction force, the force applied to the crosshead (related to the force applied to the powder column by the upper punch); F_d, die force, the force applied to the die to keep it still during compaction (related to the frictional force between the powder column and the die walls); X, the position of the lower surface of the upper punch with respect to the upper surface of the lower punch (as derived from the distance measured by two encoders fixed to the crosshead and to the base plate of the press, respectively); Z, the position of the upper surface of the die, again with respect to the upper surface of the lower punch (as derived from the distance measured by two encoders fixed to the die and to the base plate of the press, respectively) [13].

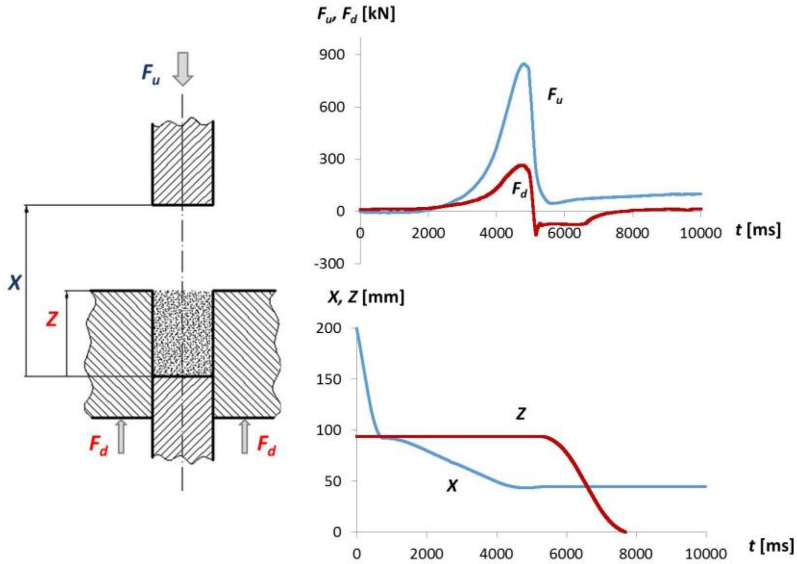

Fig. 1: Parameters recorded by the press

3. Results and discussion

3.1 Stresses on the powder column

As shown in figure 2, the forces acting on the powder column are F_u (applied by the upper punch), F_l (applied by the lower punch), and the mean frictional force F_μ (due to the relative displacement between the powder column and the die walls), which is related to the radial force F_r .

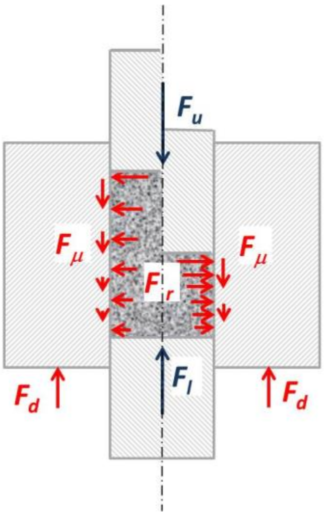

Fig. 2: Forces on the powder column

The frictional force F_μ can be directly derived from the equilibrium of forces acting on the die, as by equation (1), being F_d continuously measured by the press

$$F_d + F_\mu = 0 \tag{1}$$

Now focusing on stresses, the axial stress relevant to the force applied to the powder column can be derived from measured entities, as by equation (2)

$$\sigma_{a,u} = F_u \Big/ \pi \cdot \frac{D^2}{4} \tag{2}$$

Where F_u is the compaction force and D is the diameter of the die cavity.

The mean radial stress σ_r is related to the frictional forces by equation (3)

$$F_\mu = \mu \cdot F_r = \mu \cdot \sigma_r \cdot S = \mu \cdot \sigma_r \cdot \pi \cdot D \cdot h \tag{3}$$

Where μ is the friction coefficient between the powder column and the die walls, and S is the friction surface, which is computed by means of D, the diameter of the die cavity, and h, the actual height of the powder column determined by the position of the upper punch X, as described in previous works [9,10,12]. In this way, the entity $\mu\sigma_r$ can be derived from measured parameters, which are the frictional force (by the force applied to the die) and the friction surface.

Figure 3 shows the mean radial stress multiplied by the friction coefficient versus the upper axial stress for the different materials and geometries.

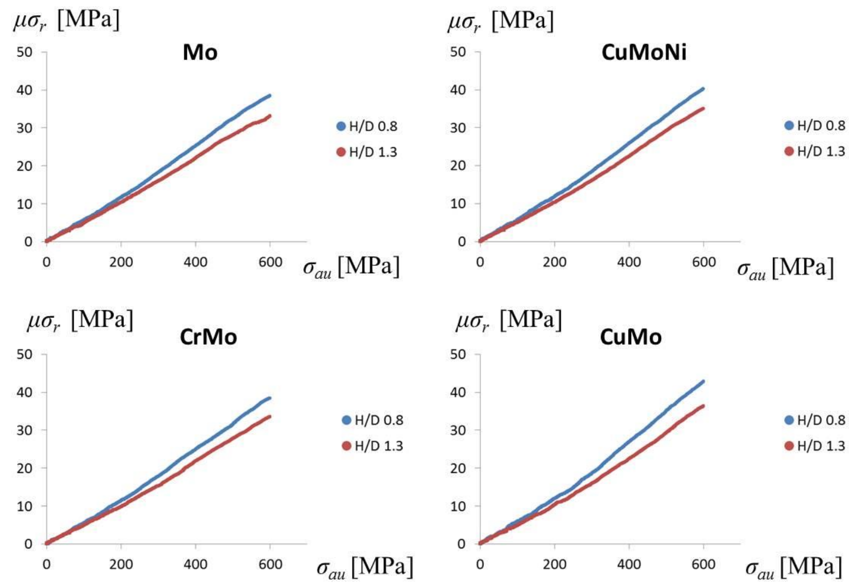

Fig. 3: $\mu\sigma_r$ vs. $\sigma_{a,u}$ for the different materials and H/D ratios

On increasing the upper axial stress, the term $\mu\sigma_r$ increases as expected. Nevertheless, different curves are observed depending on the H/D ratio for all the materials, what will be considered in the following.

Moving to the mean axial stress σ_a, the axial gradient of the compaction force is considered. The force exerted by the lower punch, F_l, is given by the equilibrium of forces acting on the powder column (see figure 2), as by equation (4)

$$F_u = F_\mu + F_l \tag{4}$$

F_l is also related to the mean axial and radial stresses by equation (5)

$$F_l = F_u \cdot e^{-4\mu\frac{\sigma_r}{\sigma_a}\frac{h}{D}} \tag{5}$$

Consequently, the mean axial stress is given by equation (6). It is worth underlining that all parameters are known, as previously highlighted.

$$\sigma_a = \frac{-4 \cdot \mu\sigma_r \cdot h}{D \cdot \ln\frac{F_l}{F_u}} \tag{6}$$

Aiming at determining the mean radial stress σ_r, the friction coefficient μ needs to be investigated. The friction coefficient can be obtained by the theoretical relationships between the mean radial stress σ_r and the mean axial stress σ_a, given by equations (7) and (8), in the elastic and plastic field, respectively

$$\sigma_r = \sigma_a \cdot \frac{\nu}{1-\nu} \tag{7}$$

$$\sigma_r = \sigma_a - \sigma_f \tag{8}$$

Where ν is the Poisson's coefficient, and, according to the Tresca yield criterion, σ_f is the flow stress of the powder, which increases continuously during compaction due to densification and strain hardening of the metallic powder. The densification curves for the different materials, reporting the relative density versus the mean axial stress, show that the transition point corresponds to $\rho_r \approx 0.78$ for materials Mo, CuMoNi, and CuMo, and to $\rho_r \approx 0.73$ for CrMo [14].

Assuming ν=0.25 [15], the friction coefficient in the elastic field can be derived by equation (7) simply multiplying the terms by μ, obtaining equation (9)

$$\mu = \frac{\mu\sigma_r \cdot (1-\nu)}{\sigma_a \cdot \nu} \tag{9}$$

Figure 4 shows the friction coefficient versus the relative density for the different materials and H/D ratios. The highly scattered and poorly interesting values corresponding to relative density lower than 0.63 have been neglected.

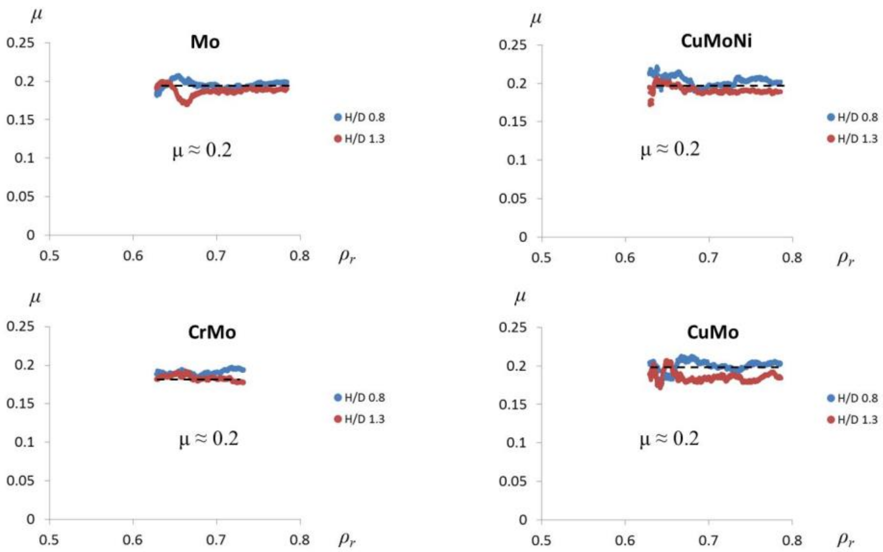

Fig. 4: μ vs. ρ_r for the different materials and H/D ratios

For each material and H/D ratio, in the considered field μ is almost constant around the value 0.2. In the plastic field the friction coefficient is expected to be constant, as from the literature [5]. The relationship between mean axial and mean radial stress is given by equation (8), from which, combining equations (3) and (6), equation (10) describing the flow stress σ_f is obtained

$$\sigma_f = \sigma_a - \sigma_r = \frac{-4 \cdot \mu\sigma_r \cdot h}{D \cdot \ln \frac{F_l}{F_u}} - \frac{F_\mu}{\mu \cdot \pi \cdot D \cdot h} \tag{10}$$

In this equation the friction coefficient is the only unknown parameter, so that different values have been hypothesized. Figure 5 shows the flow stress vs. the relative density for the different materials and H/D ratios, calculated using different values for the friction coefficient.

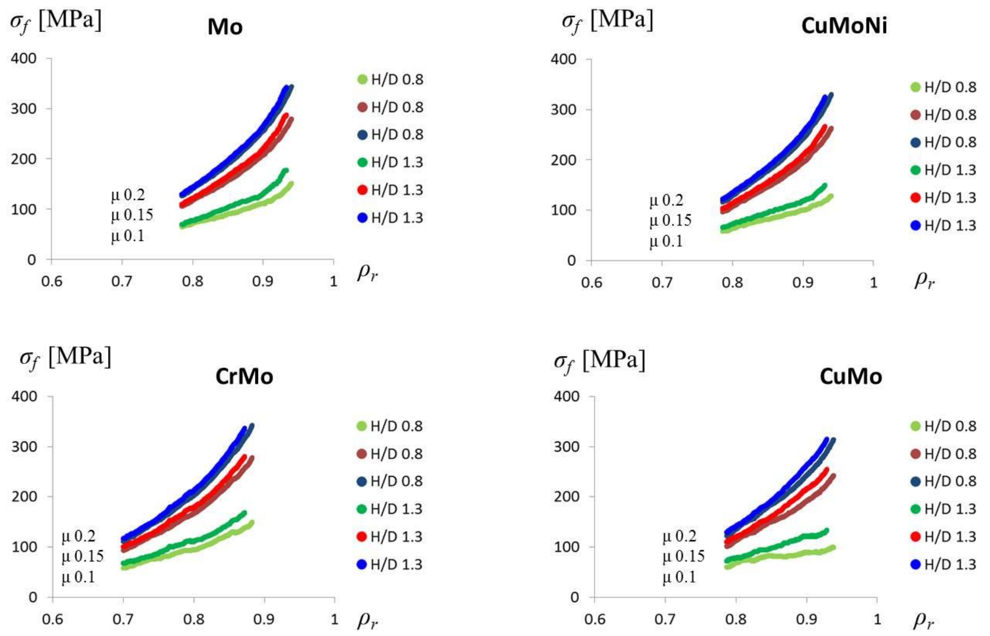

Fig. 5: σ_f vs. ρ_r for the different materials and H/D ratios

The curves are satisfactorily fitted by equation (11)

$$\sigma_f = \sigma_{f0} \cdot \rho_r^{\,b} \tag{10}$$

σ_{f0} represents the flow stress at the theoretical density, which is a (purely theoretical) intrinsic characteristic of the powder used, irrespective of the H/D ratio. This is why the friction coefficient, which leads to the best overlapping of the curves for the different H/D ratios, has been chosen, for each material, as that best representing the behaviour of the powder column in the plastic field, as shown in figure 6. This value of the friction coefficient is 0.2 for all the materials, which is also the value found in the elastic field, thus further validating the approach followed.

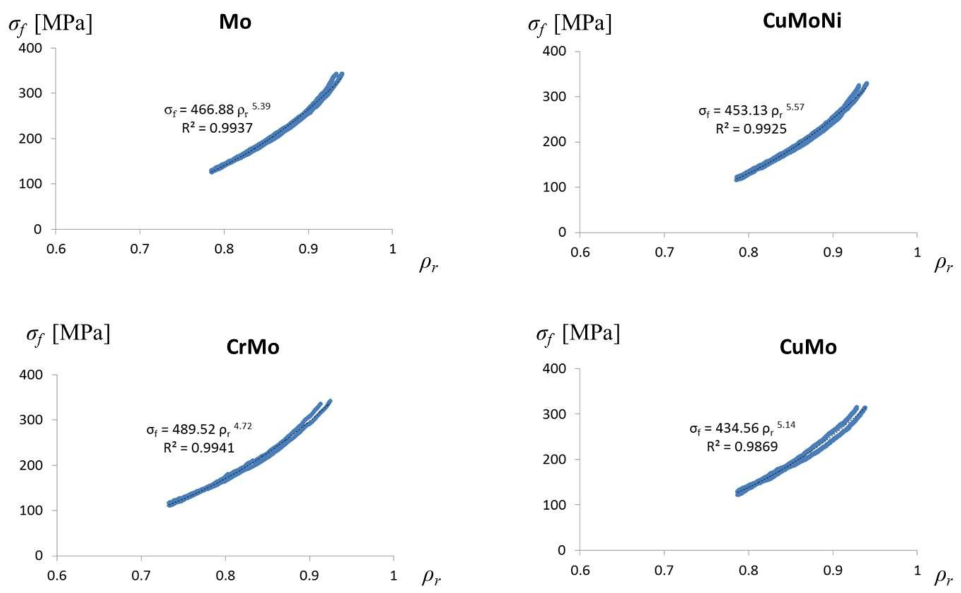

Fig. 6: σ_f vs. ρ_r for the different materials and H/D ratios, as by μ=0.2

Nevertheless, the above result is not completely satisfactory. Indeed, the above hypothesis let expecting that all the curves tend to the same value on increasing the relative density, while they tend to diverge for the different H/D ratios, if the same friction coefficient is considered for all the geometries. The friction coefficient shown in figure 4 is thus reconsidered. If the data related to the different H/D ratios are separately evaluated, for all the materials two slightly but distinctly different friction coefficient can be identified for the different geometries. They are summarized in Table 2.

Table 2: Friction coefficient for the different materials and geometries

	μ	
	H/D 0.8	**H/D 1.3**
Mo	0.20	0.19
CuMoNi	0.20	0.19
CrMo	0.19	0.18
CuMo	0.20	0.19

The slightly lower friction coefficient, which in all the materials is observed for the highest H/D ratio, might be due to the better efficiency of the lubricant in the higher specimens. The frictional heat due to the sliding of the powder particles against the die walls is in fact reasonably supposed to be larger for the highest specimens, due to the higher sliding distance covered by the powder particles. As a consequence, the efficiency of the lubricant, which increases on increasing the temperature, is improved. It has to be underlined that, despite of the of the slightness of the differences, when processing all the data using a unique, intermediate value, the flow stress curves for the two H/D ratios still tend to diverge. From here on, the analysis will use the values shown in Table 2 for the friction coefficient. As a first consequence, the flow stress curves shown in figure 7 are overlapped.

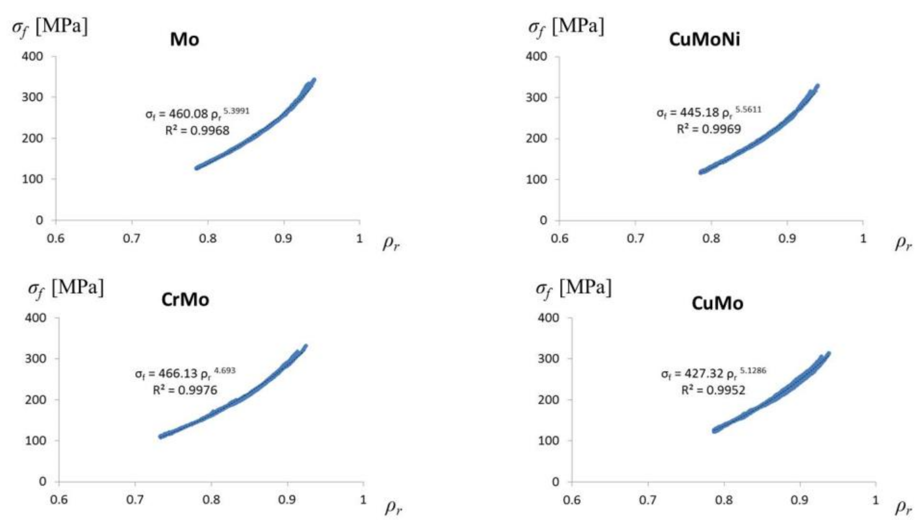

Fig. 7: σ_f vs. ρ_r for the different materials - specific friction coefficients for each H/D ratio

The model for the flow stress is almost the same for three materials, as shown in figure 8.

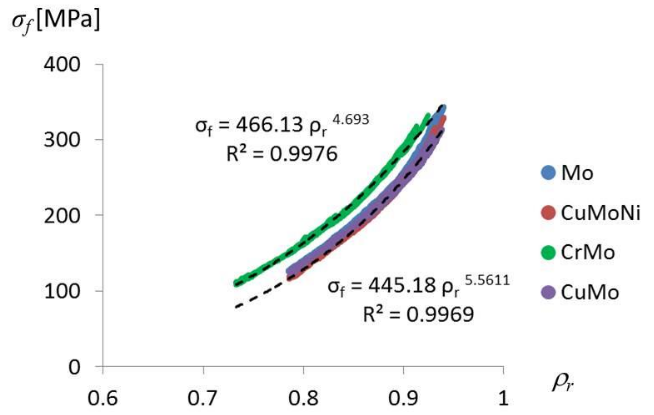

Fig. 8: σ_f vs. ρ_r - different materials gathered

Only CrMo differs from the others, being the flow stress evidently higher. This may be related to the higher amount of pre-alloyed elements, which increases the resistance to plastic flow.

The mean axial and radial stresses can be finally derived, and, when plotted versus the relative density, same trend is observed (see figure 9).

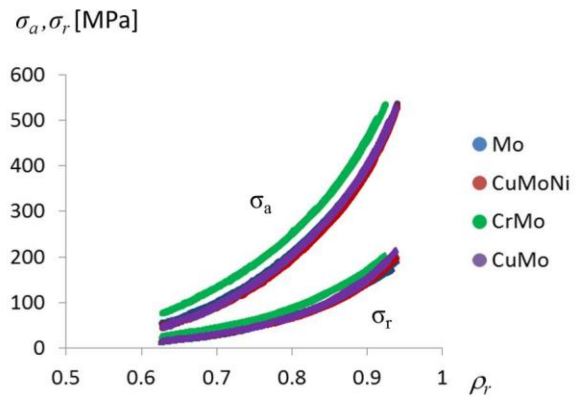

Fig. 9: σ_a and σ_r vs. ρ_r - different materials gathered

Again CrMo differs from other materials, showing higher axial and radial stresses at the same relative density. Moreover, for all the materials the mean axial stress is higher than the mean radial stress every relative density, as expected, and the difference is even larger on increasing the relative density, that is on increasing plastic deformation. However, the ratio between the mean axial and mean radial stresses gives even more interesting information.

The radial stress transmission coefficient $K = \sigma_r / \sigma_a$ is derived from the mean axial and radial stresses, as shown in figure 10 for the different materials as a function of the relative density.

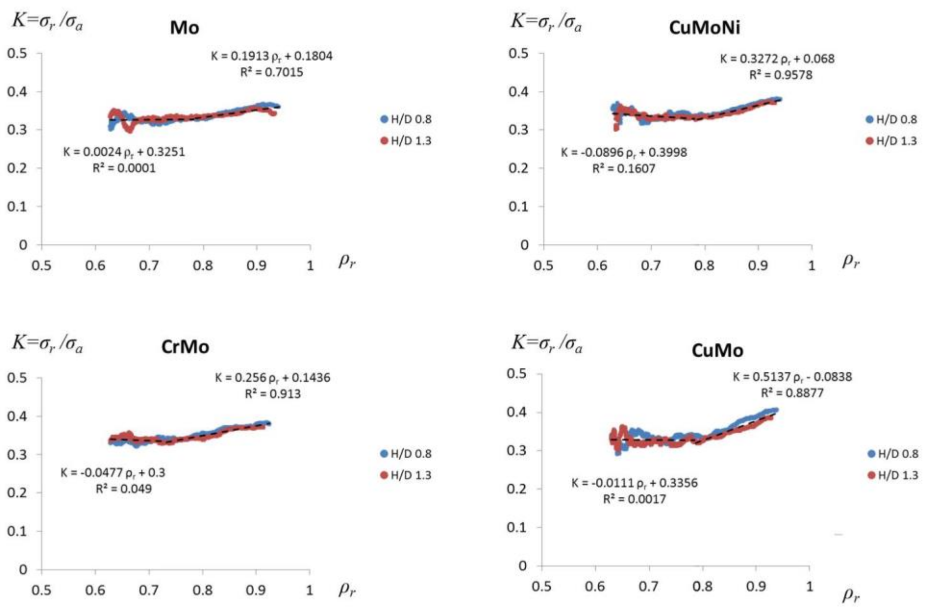

Fig. 10: K vs. ρ_r for the different materials and H/D ratios

For all the materials two distinct relationships can be found, corresponding to prevailing elastic or plastic deformation. In both ranges the radial stress transmission coefficient is almost constant in the elastic field, while it increases with the relative density in the plastic field. Gathering the data for all the materials, no significant differences are observed in the elastic field; in the plastic field the slight difference already observed for the CrMo is confirmed, as shown in figure 11.

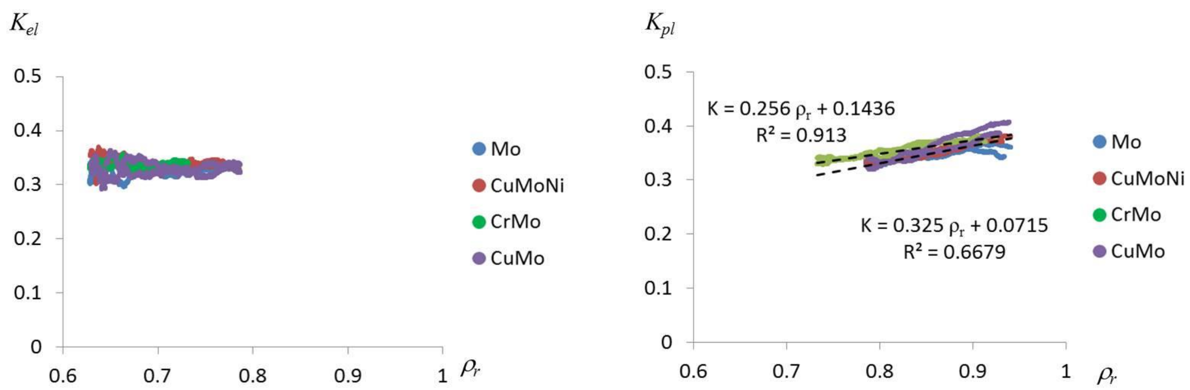

Fig. 11: K vs. ρ_r in the elastic and plastic field - different materials gathered

The analysis above has been performed under the hypothesis of a given value for the Poisson coefficient (ν=0.25). The hypothesis can now be validated by means of the radial stress transmission coefficient $K=\sigma_r/\sigma_a$ and the relationship between the axial and radial stress in the elastic field (eq. 7), leading to equation (11)

$$\nu = \frac{K}{1+K} \tag{11}$$

Figure 12 shows for the different materials the Poisson coefficient as a function of the relative density derived from equation (11), which validates the hypothesized value ν=0.25.

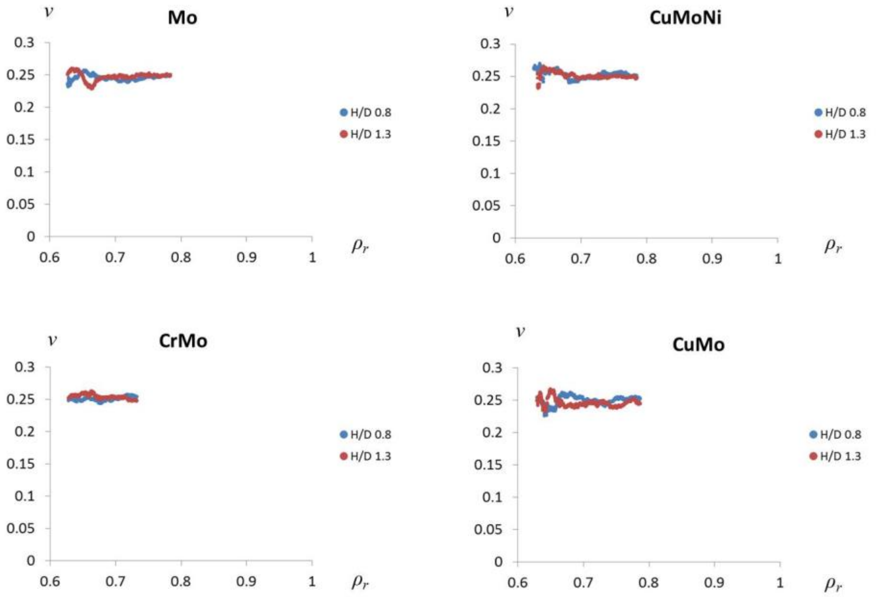

Fig. 12: ν vs. ρ_r in the elastic field for the different materials

3.2 Young modulus *E*

Aiming at giving a complete description of the parameters characterising the behaviour of the powder column during uniaxial cold compaction, Young modulus has to be identified. Young modulus is expected to be anisotropic [16], and it can be derived from the Hooke stress/strain relationships described by equations (12) and (13)

$$\varepsilon_a = \frac{\sigma_a}{E_a} - 2\nu\frac{\sigma_r}{E_r} \tag{12}$$

$$\varepsilon_r = \frac{\sigma_r}{E_r} - \nu\frac{\sigma_a}{E_a} - \nu\frac{\sigma_r}{E_r} \tag{13}$$

As long as the powder is inside the die, ε_r=0 due to constrain exerted by the die, the elastic deformation of which is supposed to be negligible. Under this hypothesis, equations (14) and (15) derive from (12) and (13)

$$E_a = \frac{\sigma_a}{\varepsilon_a}\cdot\frac{1-\nu-2\nu^2}{1-\nu} \tag{14}$$

$$E_r = E_a\cdot\frac{\sigma_r}{\sigma_a}\cdot\frac{1-\nu}{\nu} \tag{15}$$

The axial strain, which is needed to calculate the axial Young modulus, can be derived from the unloading step of the compaction curves. Experiments were performed at different levels of compaction force and the reversible displacements were derived from the compaction curves, as described in [12]. The axial strain was obtained by the reversible displacement corresponding to the maximum height of the powder column fully contained within the die during unloading, as by the scheme in figure 13.

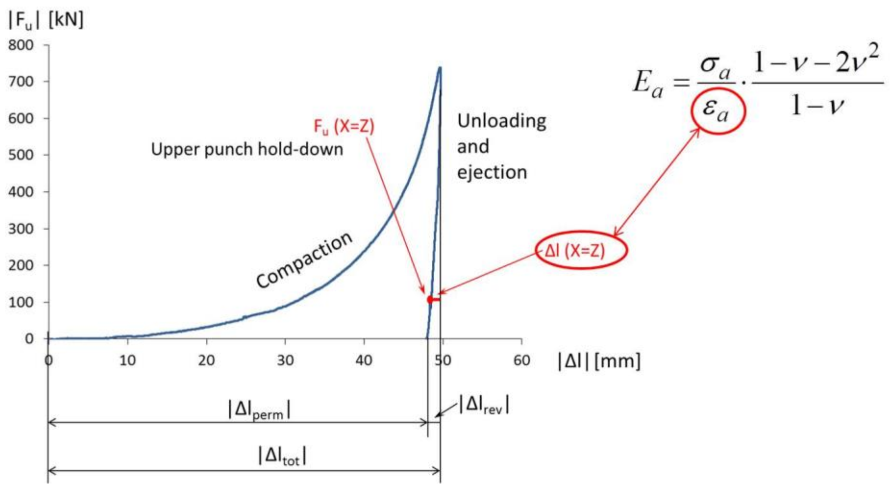

Fig. 13: Example of compaction curve

Problem is that the unloading step of the compaction curves is very steep, so that the reversible displacement is extremely small, (once subtracted the contribution of the elastic displacement of the tool [12]), and even more the elastic strain, so that the derived Young moduli are not sufficiently reliable. However, elastic axial and radial strains can also be obtained considering the spring-back of the green parts, due to the recovery of the elastic deformation. The dimensions of the green parts have been measured and the elastic axial and radial strains have been derived, as by equations (16) and (17)

$$\varepsilon_a = \frac{h_g - h}{h} \tag{16}$$

$$\varepsilon_r = \frac{D_g - D}{D} \tag{17}$$

Where *h* is the height of the powder column at the maximum compaction force and *D* is the diameter of the die cavity. Introducing the axial and radial strains above in equations (12) and (13), the axial and radial Young moduli are derived.

Strictly speaking, equations (16) and (17) define relationships between dimensions during compaction (inside the die) and after compaction (outside the die), and the derived entities are actually representative of strains only if no change in density occurs. Both the density of the powder column inside the die at the maximum compaction force and the green density of the part outside the die have been calculated, and the difference between them has been computed to be less than 1% [14]. This difference has been considered as negligible, and the axial and radial strains obtained from equations (16) and (17) have been used to derive the axial and radial Young moduli shown in figure 14 for the different materials. No data related to relative density lower than 0.7 are reported due to the insufficient strength of the green parts, which did not allowed obtaining reliable measurements.

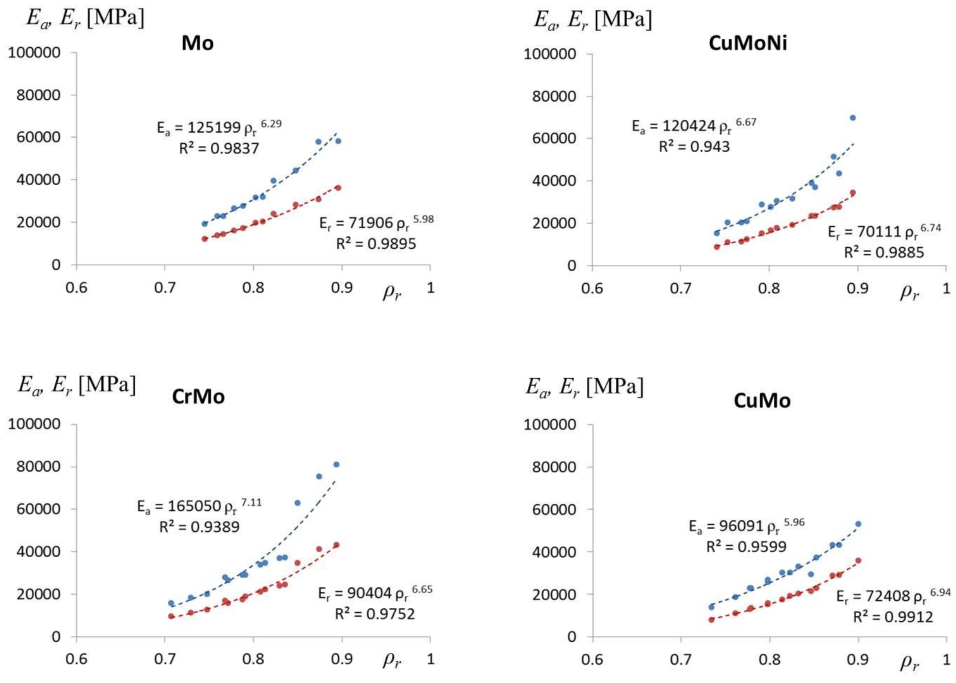

Fig. 14: Axial and radial Young moduli vs. the relative density for the different materials

The difference between CrMo material and the other materials (quite similar among them) is again confirmed. As expected, the difference between axial and radial Young moduli increases on increasing relative density, that is on increasing the anisotropic plastic deformation. Young moduli in figure 15 might appear quite small, when compared to the Young moduli of the correspondent steels, but is has to be underlined that the entities above represent the Young moduli of the powder column, which means a mixture of powder particles, lubricant, graphite and voids, the effect of which is large and difficult to estimate. Nevertheless, green parts come from the powder column, so that the related parameters have to be considered in the design step.

4. Conclusions

The behaviour of four different commercial water atomized low alloyed powders during uniaxial cold compaction was investigated in this work, by means of single action tests, producing specimens with different H/D ratios (0.8 and 1.3). For all the materials the stress field acting on the powder column has been studied, also identifying how it affects the parameters determining the densification. The main results are summarized as follows:

- The friction coefficient between die walls and powder column is almost the same for all the materials in the whole range of relative density investigated ($\mu \approx 0.2$). Nevertheless, slight differences in the friction coefficient have been highlighted for the different H/D ratios, for all the materials. A deeper analysis highlighted that such slight differences have to be taken into account to furtherly improve the description of powder behaviour. The slightly lower friction coefficient, which in all the materials is observed for the highest H/D ratio, might be related to the frictional heat due to the sliding of the powder particles against the die walls, which is reasonably supposed to be larger for the highest specimens, thus determining the better efficiency of the lubricant.

- The stress field acting on the powder column has been described for all the materials as a function of the relative density, by different relationships depending on the predominance of the elastic or plastic deformation. The radial stress transmission coefficient is almost constant in the elastic field, while it tends to linearly increase on increasing the relative density, when plastic deformation prevails. The trend is described by similar relationships for all the materials, except for the CrMo, showing a higher increase, which might be due to the largest amount of prealloyed elements.
- Same different behaviour for CrMo is highlighted by the flow stress, the dependency from the relative density of which is described by power law relationships.
- The hypothesized value of Poisson coefficient (ν=0.25) has been confirmed by the whole analysis for all the materials.
- The axial and radial Young moduli have been derived from the spring-back analysis. Increasing the relative density, which means increasing plastic deformation of powder particles, the difference between the axial and the radial Young moduli increases, and same occurs for the difference between mean axial and mean radial stresses. This result is in good agreement with the prevailing plastic deformation of the powder particles observed in the axial direction.

All these results have been obtained processing the data continuously recorded by an industrial hydraulic press, so that they represent the actual conditions in the production of real parts. Therefore these results have a noticeable practical interest, and can be used to model the compaction process for the production of parts with the same powder mixes of the present work.

References

1. S. Turenne, C. Godere, Y. Thomas, P. E. Mongeon, Evaluation of friction conditions in powder compaction for admixed and die wall lubrication, Powder Metall 42(3) (1999) 263-268
2. H. A. Al-Qureshi, A. Galiotto, A. N. Klein, On the mechanics of cold die compaction for powder metallurgy, J Mater Process Tech, 166 (2005) 135-143
3. H. A. Al-Qureshi, M. R. F. Soares, D. Hotza, M. C. Alves, A. N. Klein, Analysis of the fundamentals parameters of cold die compaction of powder metallurgy, J Mater Process Tech, 199 (2008) 417-424
4. P. Mosbah, D. Bouvard, E. Ouedraogo, P. Stutz, Experimental techniques for analysis of die pressing and ejection of metal powder, Powder Metall 40(4) (1997) 269-277
5. B. Wikman, H. A. Haggblad, M. Oldenburg, Modelling of powder-wall friction for simulation of iron powder pressing, Proceedings International Workshop on “Modelling of metal powder forming process”, Grenoble, France, 1997, 149-157
6. B. Wikman, N. Solimannhezad, R. Larsson, M. Oldenburg, H. A. Haggblad, Wall friction coefficient estimation through modelling of powder die pressing experiment, Powder Metall 43(2) (2000) 132-138

7. E. Pavier and P. Doremus, Friction behaviour of an Iron Powder Investigated with Two Different Apparatus, Proceedings International Workshop on “Modelling of metal powder forming process”, Grenoble, France, 1997, 335-344
8. E. Pavier, P. Doremus, Triaxial characterisation of iron powder behaviour, Powder Metall, 42 (4) (1999) 345-352
9. I. Cristofolini, A. Rambelli, G. Pederzini, A. Molinari, Study of the uniaxial cold compaction of AISI 316L stainless steel powders through single action tests, Powder Technol, 295 (2016) 284-295
10. I. Cristofolini, G. Pederzini, A. Rambelli, A. Molinari, Study of the Behaviour of Low Alloy Steel Powder during Uniaxial Cold Compaction by means of Single Action Tests, in Proceedings WorldPM2016 – Powder Pressing, (2016)
11. PM Modnet Methods and Measurement Group, Measurements of friction for powder compaction modelling – comparison between laboratories, Powder Metall 43(4) (2000) 364-374
12. I. Cristofolini, A. Molinari, G. Pederzini, A. Rambelli, Stress distribution and densification in unaxial cold compaction – from experiments to mechanics relationships, Advances in Powder Metallurgy & Particulate Materials-2016, 1 (2016) 34-44
13. I. Cristofolini, A. Rambelli, G. Pederzini, A. Molinari, Densification and deformation during unixial cold compaction of stainless steel powder with different particle size, Powder Metall, 59(1) (2016) 73-84
14. A. Molinari, I. Cristofolini, G. Pederzini, A densification equation for low alloy steel powder mixes in uniaxial cold compaction based on deformation caused by the compaction pressure, submitted to Powder Metall
15. C.L. Martin, Elasticity, fracture and yielding of cold compacted metal powders, J Mech Phys Solids, 52 (2004) 1691-1717
16. P. C. Carnavas and N. W. Page, Elastic properties of compacted metal powders, J Mater Sci 33 (1998) 4647-4655

Figure captions

Fig. 1: Parameters recorded by the press

Fig. 2: Forces on the powder column

Fig. 3: $\mu\sigma_r$ *vs.* $\sigma_{a,u}$ *for the different materials and H/D ratios*

Fig. 4: μ *vs.* ρ_r *for the different materials and H/D ratios*

Fig. 5: σ_f *vs.* ρ_r *for the different materials and H/D ratios*

Fig. 6: σ_f *vs.* ρ_r *for the different materials and H/D ratios, as by* μ*=0.2*

Fig. 7: σ_f *vs.* ρ_r *for the different materials - specific friction coefficients for each H/D ratio*

Fig. 8: σ_f *vs.* ρ_r *- different materials gathered*

Fig. 9: σ_a *and* σ_r *vs.* ρ_r *- different materials gathered*

Fig. 10: K *vs.* ρ_r *for the different materials and H/D ratios*

Fig. 11: K *vs.* ρ_r *in the elastic and plastic field - different materials gathered*

Fig. 12: ν *vs.* ρ_r *in the elastic field for the different materials*

Fig. 13: Example of compaction curve

Fig. 14: Axial and radial Young moduli vs. the relative density for the different materials